# Stochastic modeling of gob gas venthole production performances in active and completed longwall panels of coal mines

C. Özgen Karacan [a,*], Kray Luxbacher [b]

[a] NIOSH, Office of Mine Safety and Health Research, Pittsburgh, PA, United States
[b] Virginia Tech, Dept. of Mining and Minerals Engineering, Blacksburg, VA, United States

A B S T R A C T

Gob gas ventholes (GGVs) are an integral part of longwall coal mining operations, enhancing safety by controlling methane in underground workings. As in many disciplines in earth sciences, uncertainties due to the heterogeneity of geologic formations exist. These uncertainties, and the wide range of mining and venthole operation parameters, lead to performance variability in GGVs. Random variations in parameters affecting GGV performance and influencing parameters that cannot be quantified sufficiently due to lack of information limit deterministic GGV models and even introduce error in severe cases. Therefore, evaluation of GGV performance data and the uncertainty in input parameters is valuable for understanding the variability in GGV production and for designing them accordingly.

This paper describes a practical approach for implementing stochastic determination of GGV production performances and for generalizing the prediction capability of deterministic models. Deterministic site-specific models were derived by using the GGV module in the recently developed MCP (Methane Control and Prediction) software suite. These models were generated using multi-parameter regression techniques and were then improved by inclusion of extra input parameters that eliminated the site dependency and improved the predictions. Statistical distributions of input parameters in these models were quantified and tested with the Kolmogorov–Smirnov goodness-of-fit technique. Next, Monte Carlo simulations were performed using these distributions and generalized results for GGV performances were generated. The results of this work indicate that this approach is a promising method of representing the variability in GGV performances and to improve the limited and site-specific character of the deterministic models.

## 1. Introduction

Longwall gobs have high-permeability fractures that form open pathways for gas transport towards the mining environment, making them prime targets for gas control measures. Drilling vertical gob gas ventholes (GGVs), which begin to vent gas as the longwall face advances under their locations, is an effective technique for capturing methane emissions within the overlying fractured strata before they enter the work environment. The challenges involved in testing, characterizing, modeling, and evaluating the reservoir properties of the gob make it difficult to evaluate the performance and productivity of GGVs and to design GGVs for the maintenance of underground health and safety in the face of high methane emissions.

Characterization of the fractured zone and determination of its reservoir properties are complicated. Because measured data are scarce and formation deformation during subsidence is complex, it is difficult to set up a numerical model of the gob for flow simulations. Previously, Lunarzewski (1998) used boundary element and sequential bed separation methods for floor and roof strata relaxation and immediate roof bending separation in addition to gas emission rate calculations. Ren and Edwards (2002) used a computational fluid dynamics (CFD) modeling approach to investigate gas capture from surface GGVs. That paper introduced the use of CFD approach to improve the design of surface gob wells for methane recovery while minimizing the leakage of air into the gob. Tomita et al. (2003) developed a three-dimensional (3-D) finite element model (FEM) to predict the volume of methane gas emitted from surrounding coal and rock layers based on stress distribution and permeability changes. Geomechanical modeling is used to simulate the complex permeability, porosity, and elastic property changes that take place with the fracturing of overburden strata, formation and recompaction of gob, and desorption of methane from intact reservoirs. Esterhuizen and Karacan (2007) coupled geomechanical modeling with reservoir modeling, and Kelsey et al. (2003) coupled geomechanical modeling with CFD to model drainage through the strata around longwall gob. CFD is a robust method, but also computationally expensive,

Disclaimer: The findings and conclusions in this report are those of the authors and do not necessarily represent the views of the National Institute for Occupational Safety and Health. Commercial software mentioned in this paper is not endorsed by NIOSH.

* Corresponding author. Tel.: +1 412 386 4008; fax: +1 412 386 6595.
*E-mail address:* cok6@cdc.gov (C.Ö. Karacan).

especially for large scale, complex models, such as the longwall gob. However, it can be used to understand the mechanisms governing desorption and flow at micro- and macro-levels. Traditional reservoir simulation, which can be accomplished with several numerical methods, can also prove computationally expensive, and is primarily used to understand the influence of reservoir and well parameters, and forecast long term production. The two methods complement each other by allowing for characterization of the mechanisms that induce and influence flow, while also allowing for production optimization.

In order to address some of the difficulties in modeling in a more practical way, Karacan (2009a) developed an artificial neural network (ANN)-based model using field data to predict GGV production rates and methane concentrations. The total gas productions and methane percentages of 10 ventholes located over 3 adjacent panels in the southwest Pennsylvania section of the Northern Appalachian basin were monitored at the wellhead using pressure, flow, temperature, and methane sensors. The monitoring took place for more than 2 years, both during and after mining of these panels. The measurements, along with various spatial parameters related to venthole location, borehole completion parameters, mining rate and panel completion data, and exhauster operation data, were combined to form an extensive database. The ANN model was successful in predicting methane percentage and production rate with a correlation coefficient, R, greater than 0.9. Sensitivity analyses about the mean of the input variables were conducted using the ANN model to identify which input variables had more influence on the performance of GGVs.

Because methane production from a GGV can often be characterized as an event with multiple episodic phenomena controlled by numerous variables associated with uncertainty and randomness, deterministic methods of evaluation and their results may not always be satisfactory. Stochastic methods, such as Monte Carlo, can support deterministic methods. Monte Carlo (MC) methods produce an approximation by calculating results from a large number of random samples within the test domain.

General Monte Carlo methods have been proven a useful tool for accurately estimating statistical uncertainties in standard errors and confidence intervals in non-linear regression problems (Alper and Gelb, 1990), and are applied frequently in studying particle physics and in nuclear engineering (Haghighat and Wagner, 2003) to obtain a probabilistic solution to a deterministic problem. MC methods are also used in porous media flow and transport problems for ground water contamination and remediation studies. Huang et al (2003) applied MC methods to study groundwater flow and solute transport in heterogeneous, dual-porosity media and compared the results with analytical models. Morin and Ficarazzo (2006) used stochastic techniques and MC simulations to predict fragmentation of rock during blasting. They have shown that the results produced by the simulator were comparable with the data obtained from a quarry, and that the use of MC extended the understanding of the factors affecting blast fragmentation. Sari (2009) demonstrated the use of MC simulations to evaluate the strength and deformability of rock masses by including the uncertainties of the intact rock strength and discontinuity parameters. He concluded that the MC method provided a viable means for assessing the variability of rock mass properties. Lu and Zhang (2003) demonstrated the development of an important sampling method to solve complicated problems with MC and applied it to fluid transport problems in aquifers.

This paper describes a practical approach for implementing stochastic determination of GGV production performances and for generalizing the prediction capability of deterministic models. For this approach, deterministic models were derived by using the GGV module in the recently developed MCP (Methane Control and Prediction) software suite (Karacan, 2010) and generalized to remove site-specificity. Statistical distributions of input parameters in these models were quantified and tested for goodness of fit. Monte Carlo simulations were performed using these distributions and the generalized deterministic models to assess the variability of GGV production rates and methane percentages. While CFD and reservoir simulation, coupled with geomechanical modeling can realistically simulate the physics of single and multiphase flow they require considerable knowledge of the reservoir, and significant computational time and expense. The approach presented here provides a relatively fast estimation of performance for a single point in time and space.

## 2. Approach to deterministic modeling of production rates and methane concentrations

### *2.1. A brief introduction to Methane Control and Prediction (MCP) software suite*

The MCP software suite was developed to provide proxy solutions to some of the problems related to controlling and capturing methane from longwall mines. The software suite consists of dynamic link library (DLL) extensions to MS-Access™, written in C++ and using various mathematical approaches and artificial neural network (ANN) methods.

The first version of MCP contains four main modules:

- Coal measure rock mechanical properties prediction. Predicts dynamic elastic properties of coal-measure rocks for better roof support and methane control.
- Mine ventilation emission prediction. Predicts ventilation air methane (VAM) emissions from longwall mines.
- Degasification system selection. Recommends the best degasification choice for a given mine design, operational conditions, and targeted VAM conditions.
- Gob gas venthole production performance prediction. Predicts performance of GGVs in terms of total production rate and methane concentration.

These models produce the desired predictions with known basic log, mining, longwall panel, productivity, and coal bed characteristics as input parameters. The application of these modules separately or in combination for methane capture- and control-related problems can improve the safety of coal mines. The theory and technical aspects of developments of these software modules are given in detail in Karacan (2008, 2009a,b,c), and the software suite is available for download from http://www.cdc.gov/niosh/mining/products/product180.htm free of charge (Karacan, 2010).

Details of MCP and its possible applications are given in Dougherty and Karacan (in press). This current paper deals with the deterministic and stochastic approaches to the prediction of GGV performance. Readers are referred to Karacan (2009a) for the details of development of the GGV module and for a detailed discussion of input parameters and their influences on production performances.

Fig. 1 shows two screen captures from the input parameter screen of the GGV module in the MCP software suite. This screen requires information on the status of the longwall panel, either active or completed (Fig. 1-A), and on the status of longwall face, as advancing or idle (Fig. 1-B). Other inputs include those related to borehole drilling, completion, mine layout, mine operation and operation of an exhauster at the surface. The module will generate prediction for two panel and face situations: *an advancing panel and active face (A-A)* or *a completed panel and idle face (C-I)*. The A-A and C-I abbrevations will be used throughout the rest of this paper to designate the two circumstances that are common to the operation of gob gas ventholes: when the mine is active (A-A), and after the panel is completed and/or abandoned (C-I).

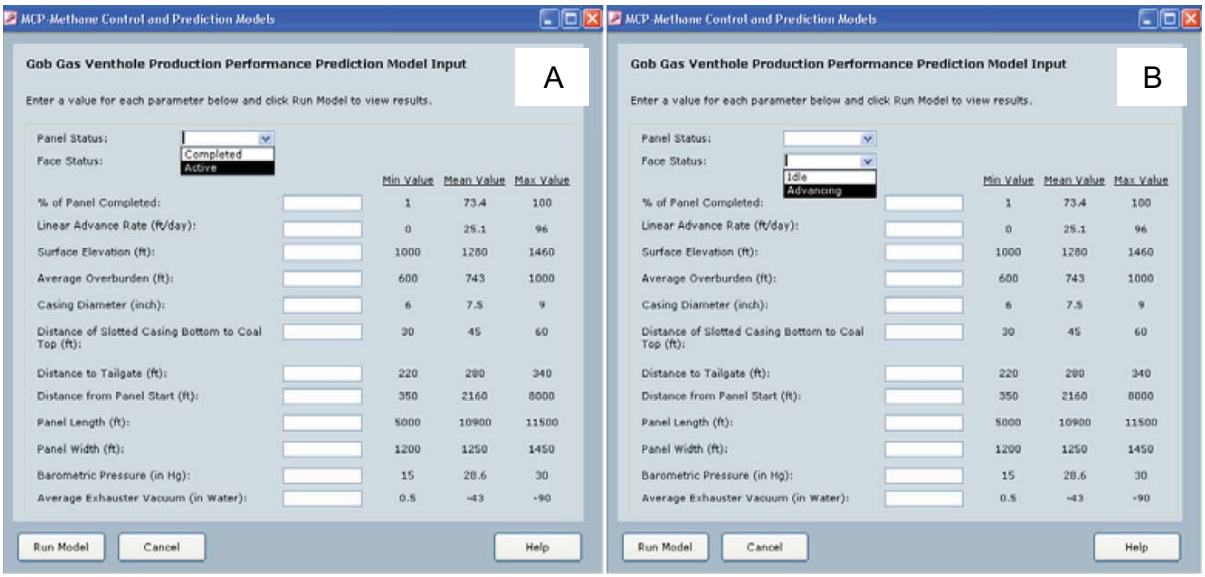


**Fig. 1.** GGV module input screens that show common input parameters and the selections for panel status (A) and longwall face status (B).

### *2.2. The use and application of the GGV production performance prediction model for deterministic modeling*

The GGV production performance prediction module in the current version of the MCP calculates GGV total gas production rates and the methane concentrations in the produced gas stream. The various input parameters are complex, and since the original ANN model was developed using the field data obtained from the Northern Appalachian basin (Karacan, 2009a), in some cases the parameters are site-specific.

ANNs are adaptable deterministic systems that deliver one output for a given set of inputs. They can determine relationships between different sets of data to solve problems where conventional deterministic models are inefficient or insufficiently accurate. Such problems are usually complex and difficult to describe mathematically. Although the key advantages of neural networks are their abilities to recognize patterns between input and output space and to generalize solutions, the inherent disadvantage is that ANNs usually do not offer a deterministic mathematical model that shows the relations between inputs and outputs explicitly. In that respect, they can be considered as "black-box" models (Maier and Dandy, 2000).

In this study, MCP's GGV performance prediction model was used to develop proxy deterministic models for predicting methane concentration and production rates. The proxy models quantify the sensitivity of the production rate and methane concentration for different mining and GGV parameters, and describe the performance of GGVs with the range of input parameters that were used to develop the original ANN model. Using these proxy models as the basis for developing a stochastic approach allows for the statistical uncertainty that is associated with each input parameter, for the addition of input parameters, and for generalization of the site-specific nature associated with some of the input parameters to an extended range of situations. This approach eventually broadens the applicability of the stochastic models to more general situations compared to the deterministic models.

In order to obtain proxy deterministic models, the GGV performance prediction model was used to generate flow rate and methane concentration output for A-A and C-I situations. Random number generation between minimum and maximum limits of each input parameter provided the values for the input parameters. These limits were based on measured well data. For each of the A-A and C-I cases, approximately 150 input–output patterns were generated. In this study, one of the original input parameters in the A-A case, "% of panel completed," was replaced with a new parameter called "face past the borehole location" (Table 1). This new parameter gives a true measure of how far the face advanced compared to the borehole location and also ensures that the GGV is operational at that face location. This parameter is calculated as the difference of distance of the borehole from panel start minus the product of the percent panel completed and the panel length.

The input–output patterns were analyzed with multiple linear regression in order to create a reasonably accurate and easy to manipulate deterministic model for use in the stochastic approach. Since the input values were known within a reasonable range, no elimination procedures were necessary on the generated data. All of the inputs and their contributions to the variance in the models were maintained.

Fig. 2-A and B gives the results for methane percentages obtained from the MCP software plotted against those predicted by the proxy models for A-A and C-I cases, respectively. As seen from these plots, the data scatter around the coefficient of determination line, $R^2 = 1$, within one standard deviation (shown by the gray lines). Fig. 2-C and D shows that standardized residuals obtained by comparing MCP results with the predictions of methane percentages in A-A and C-I cases are mostly within $+/-$ 2, which indicate that there is no significant non-linearity in both cases (Devore and Peck, 2001).

Eqs. (1) and (2) represent the MCP calculations for production rate and methane concentration in the production stream respectively. Coefficients of determination ($R^2$) range from 0.69 to 0.88 and include all the input parameters of the GGV module in MCP software, as shown in Table 1. The variables "face past borehole location" and "linear advance rate" are not included as input parameters in the C-I case since panel and face are not active in this case.

$$\text{GGV Production Rate (scfm)} = P_1 \times x_1 + P_2 \times x_2 + \ldots\ldots + P_n \times x_n \quad (1)$$

$$\text{Methane (\%)} = R_1 \times y_1 + R_2 \times y_2 + \ldots\ldots + R_n \times y_n \quad (2)$$

### *2.3. Improvement of deterministic GGV performance prediction models (Table 1; Eqs. (1) and (2))*

The model given in Karacan (2009a) and the equations that are discussed in the previous section include most of the major

**Table 1**
Parameters and coefficients of multiple linear regression equations that calculate production rates and methane concentrations from GGVs for A-A and C-I cases.

| Production rate (scfm) — Case: A-A | | | | Methane concentration (%) — Case: A-A | | | |
|---|---|---|---|---|---|---|---|
| Parameter | | Coefficient | | Parameter | | Coefficient | |
| Intercept | | 0.000E + 00 | | Intercept | | 0.000E + 00 | |
| Face past BH | | | | Face past BH | | | |
| Location (ft) | $P_1$ | −2.015E−02 | $x_1$ | Location (ft | $R_1$ | 3.514E−04 | $y_1$ |
| Linear adv. rate (ft/day) | $P_2$ | 7.644E−01 | $x_2$ | Linear adv. Rate (ft/day) | $R_2$ | 1.261E−01 | $y_2$ |
| Surface elevation (ft) | $P_3$ | −3.062E−01 | $x_3$ | Surface elevation (ft) | $R_3$ | −1.505E−02 | $y_3$ |
| Average OB depth (ft) | $P_4$ | 8.949E−01 | $x_4$ | Average OB depth (ft) | $R_4$ | 6.039E−02 | $y_4$ |
| Casing diameter (″) | $P_5$ | 1.666E + 02 | $x_5$ | Casing diameter (″) | $R_5$ | −9.419E + 00 | $y_5$ |
| Slotted casing height from top of coal (ft) | $P_6$ | −4.631E + 00 | $x_6$ | Slotted casing height from top of coal (ft) | $R_6$ | 2.122E−02 | $y_6$ |
| Distance to TG (ft) | $P_7$ | −1.091E + 00 | $x_7$ | Distance to TG (ft) | $R_7$ | −2.025E−01 | $y_7$ |
| Distance from start (ft) | $P_8$ | 1.837E−02 | $x_8$ | Distance from start (ft) | $R_8$ | −1.241E−03 | $y_8$ |
| Panel length (ft) | $P_9$ | −4.366E−02 | $x_9$ | Panel length (ft) | $R_9$ | 3.491E−02 | $y_9$ |
| Panel width (ft) | $P_{10}$ | −5.221E−01 | $x_{10}$ | Panel width (ft) | $R_{10}$ | −1.262E−01 | $y_{10}$ |
| Atm. press (in Hg) | $P_{11}$ | 1.268E + 01 | $x_{11}$ | Atm. press (in Hg) | $R_{11}$ | −2.319E + 00 | $y_{11}$ |
| Ext vacuum (in water) | $P_{12}$ | −5.938E−01 | $x_{12}$ | Ext vacuum (in water) | $R_{12}$ | −3.292E−02 | $y_{12}$ |
| $R^2 = 0.81$ | | | | $R^2 = 0.88$ | | | |
| Production rate (scfm) — Case: C-I | | | | Methane concentration (%) — Case: C-I | | | |
| Parameter | | Coefficient | | Parameter | | Coefficient | |
| Intercept | | 0.000E + 00 | | Intercept | | 0.000E + 00 | |
| Surface elevation (ft) | $P_1$ | 1.256E−02 | $x_1$ | Surface −levation (ft) | $R_1$ | 9.736E−03 | $y_1$ |
| Average OB depth (ft) | $P_2$ | 1.560E−01 | $x_2$ | Average OB depth (ft) | $R_2$ | −8.627E−03 | $y_2$ |
| Casing diameter (″) | $P_3$ | 4.689E + 01 | $x_3$ | Casing diameter (″) | $R_3$ | 1.192E−01 | $y_3$ |
| Slotted casing height from top of coal (ft) | $P_4$ | 3.515E + 00 | $x_4$ | Slotted casing height from top of coal (ft) | $R_4$ | −1.239E + 00 | $y_4$ |
| Distance to TG (ft) | $P_5$ | −2.052E-01 | $x_5$ | Distance to TG (ft) | $R_5$ | −4.956E−02 | $y_5$ |
| Distance from start (ft) | $P_6$ | −2.051E-04 | $x_6$ | Distance from start (ft) | $R_6$ | 9.779E−04 | $y_6$ |
| Panel length (ft) | $P_7$ | −9.452E−03 | $x_7$ | Panel length (ft) | $R_7$ | 7.016E−03 | $y_7$ |
| Panel width (ft) | $P_8$ | −3.681E−01 | $x_8$ | Panel width (ft) | $R_8$ | −2.214E−02 | $y_8$ |
| Atm. press (in Hg) | $P_9$ | 1.827E + 00 | $x_9$ | Atm. press (in Hg) | $R_9$ | 2.504E + 00 | $y_9$ |
| Ext vacuum (in water) | $P_{10}$ | −3.384E + 00 | $x_{10}$ | Ext vacuum (in water) | $R_{10}$ | −1.058E−01 | $y_{10}$ |
| $R^2 = 0.69$ | | | | $R^2 = 0.74$ | | | |

parameters that might influence GGV production rate and methane concentration percentage. These parameters were discussed in Karacan (2009a) in detail and will not be repeated here. It is reasonable to assume that since the measured data used to develop the prediction model came specifically from the Northern Appalachian basin, some parameters that affect other basins may not be accounted for. Although most input parameters can be considered common to other basins, there are a few that better reflect the Northern Appalachian basin conditions. Furthermore, a few parameters were intentionally not included in the models, either because they did not vary or because they were not measured. It is possible that the intentionally and unintentionally excluded parameters could have influenced the observed production rates and methane concentrations. These parameters were:

- *Slotted casing length*. The monitored GGVs were drilled and completed with 200 ft of slotted casing. Therefore, this "variable" was constant and was not included as an input parameter in the models.
- *Distance to the top of slotted casing*. This information can be obtained knowing the *overburden depth, distance from bottom of slotted casing to top of mined coal bed,* and the *slotted casing length*. Since the casing length was not a variable in the models, the distance to the top of the slotted casing was not included either.
- *Strata displacements and subsidence*. The general stratigraphy in the Northern Appalachian basin is almost uniform and has characteristic formations that are present, although possibly with varying thicknesses. The effect of varying strata and their properties are potentially important for *subsidence,* or *strata displacements*. In the absence of direct measurements, subsidence information could not be included in the models as an input parameter.
- *Gas content of the overlying formations*. The coal beds above the Pittsburgh seam, believed to be the source of methane produced from the monitored GGVs in the Northern Appalachian basin, are usually ranked as high volatile bituminous. These coal beds have approximately the same amount of total gas content within the areal scale of the monitored mining field. Since there were no gas content measurements from the overlying strata for the studied GGVs, this potential variable was not included in the original models.

Because of the missing parameters and the uncertainty carried by the included parameters, the developed models are also subject to uncertainty. This makes a stochastic approach an attractive improvement method.

At this juncture, we proceed with the postulation that production rates and methane concentrations observed from the GGVs are the results of combinations of parameters, some of which could be included in the models as inputs and others that could not. Therefore, the missing inputs are embedded in the coefficients of the existing ones in Eqs. (1) and (2) (Table 1). If the missing variables can be included in the models as linear combinations of parameters, the modified equation can be fitted to the MCP predictions of production rate and methane concentration again, as in the previous section, to redetermine the coefficients to all variables in the modified equation.

The following sections describe the potential effects of slotted casing length (or distance to the top of slotted casing), strata displacement (subsidence), and gas content data on rate and methane concentration data, and how these were integrated into the deterministic equations (Eqs. (1) and (2)). Other input parameters will not be discussed here, but interested readers are referred to Karacan (2009a).

### *2.3.1. Slotted casing length/distance to top of slotted casing and flow fraction*

In gob gas ventholes, the slotted casing is the production interval along which all gas is expected to flow into the borehole. Thus, vertical variation of gas-bearing strata associated with the various lengths of

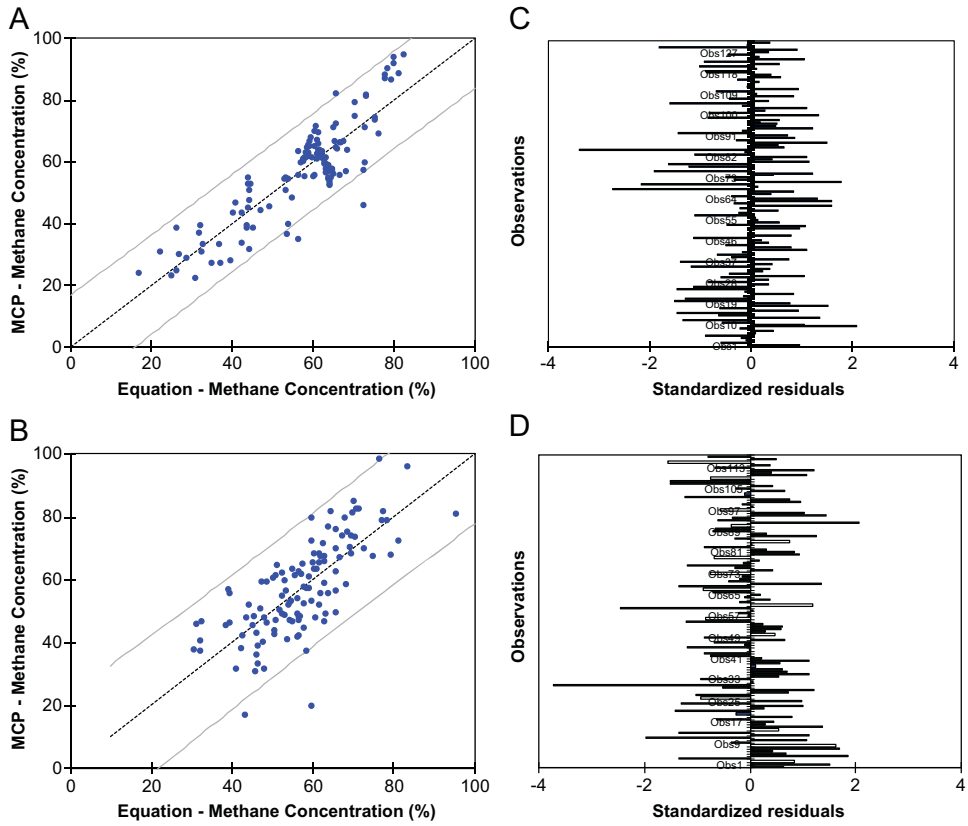


**Fig. 2.** Regression plots of methane concentration expected from the GGVs for A-A (A) and C-I (B) cases, and the standardized residuals (C and D) from these predictions, respectively.

slotted casing is expected to have a major effect on the methane production. The inclusion of coal beds, gas-bearing sandstones, and shales in the overlying strata, in the horizon of the slotted casing interval may make a significant difference in the amount of gas production. Therefore, the optimum length of slotted casing depends upon the geological layers in the overlying strata and their gas emission potentials.

Although slotted casing length can significantly affect gas production there are not sufficient field data to evaluate the effects of various lengths of slotted casing. A numerical simulation-based study investigated the changes in production performances of gob gas ventholes when the slotted casing lengths were changed to 100 ft and to 250 ft from their initial design length of 200 ft, while keeping other completion parameters constant (Karacan et al., 2007). The modeling results predicted that the cumulative methane production would increase to 459.4 MMscf with a 250-ft casing compared to 391.8 MMscf with a 200-ft casing. This represented a 9.5% increase in methane capture from the ventholes in the simulated area. When the slotted casing length was shortened to 100 ft, the predicted methane production decreased to 314.7 MMscf, an approximately 25% reduction from the 200-ft slotted casing case.

In the present study, gas flow entry locations in GGVs and the fractions of the total flow as a function of depth were used to evaluate the effect of casing length on GGV flow performance. A combined flow profile was constructed by digitizing the data from measurements of all ventholes given in Mazza and Mlinar (1977). The study was conducted in the Appalachian Basin using a data logger and a gas gun to release pulses of Kr-85 tagged nitrogen. The test system recorded the transit time of a pulse of radioactive gas along a known interval, while carried in the stream of produced gas. The velocities were then determined with the known time and distance, from which flow rates and flow percentages coming from each flow entry point in the borehole could be calculated.

Fig. 3 shows the results of the combined flow profile. Only a minor percentage of flow enters the ventholes within 50 ft of the mined coal bed. A significant increase in the flow entry occurs at approximately 175–200 ft above the mined coal seam. Between 50 and 70% of the total flow originates in this interval. As shown in Fig. 4 and discussed in the next section, this interval corresponds to the location of major displacements or strata separations in the overburden. It should be noted that this interval may not necessarily correspond to the source of the gas, but rather to the location of the major flow pathways. Almost 100% of total flow enters the GGVs by about 300–350 ft from the top of the mined coal bed.

The parameter "distance to the top of casing" can be used to include the flow entry profile in modified deterministic equations (Eqs. (1) and (2)). A new mathematical term "*distance to the top of slotted casing (D)*" was defined. Distance to top of slotted casing (D) is the average overburden depth (OB) minus the sum of slotted casing length (SL) and the distance from the bottom of the slotted casing to the top of the coal seam. This factor that modifies flow rates obtained with 200-ft slotted casing for other casing lengths. An exponential equation, $y = 41.991e^{2.0071\times}$, was fitted to the data, as shown in Fig. 3.

Flow percents (FP) that can be obtained with casing lengths other than 200 ft and the ones with 200 ft (for the same overburden and distance of the casing bottom to top of coal bed) can be defined and the flow-rate-change factor (FRF) can be calculated as:

$$FRF = \left(\frac{\ln\left(\frac{OB-D-SL}{41.991}\right)}{2.0071}\right) \Big/ FP|_{200-ft} \tag{3}$$

This equation gives a flow rate scaling factor relative to 200-ft casing length. The proposed approximation is applicable only if this

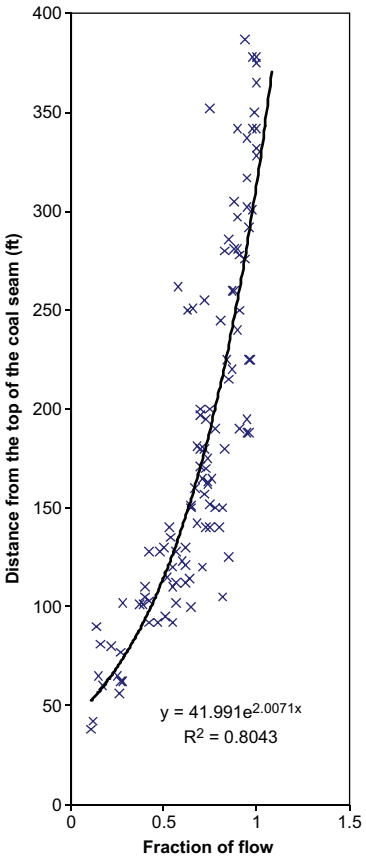


**Fig. 3.** Combined flow profiles obtained from GGVs drilled over various longwall mining operations and the exponential equation fitted to this data.

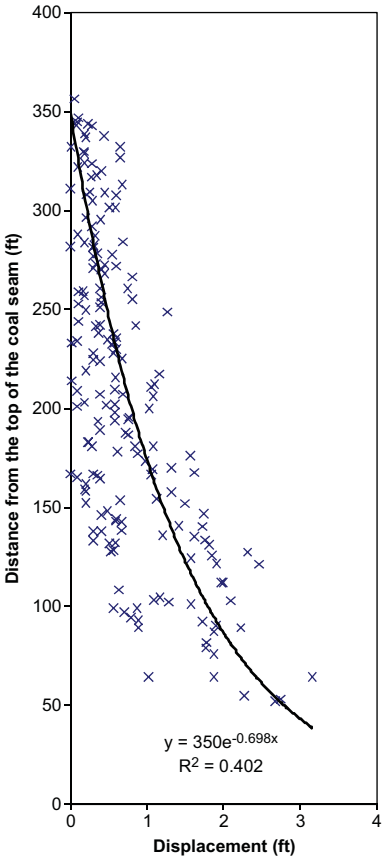


**Fig. 4.** Combined strata separations obtained from GGVs drilled over various longwall mining operations in the Northern Appalachian basin and the exponential equation fitted to this data.

factor can be calculated for given values of SL, D, and OB, including their uncertainities.

*2.3.2. Strata displacements and subsidence*

During longwall mining, vertical and horizontal fractures occur during the movement of the overburden. Horizontal fractures in the formation mostly occur along strong–weak rock layer interfaces and influence the hydraulic conductivity of the overburden strata, which creates methane emission pathways and determines methane emissions into the mine (Karacan and Goodman, 2009). The ability to estimate the locations and magnitudes of the fractures and their hydraulic flow properties is important for placement of boreholes and, consequently, for controlling methane more effectively.

Palchik (2003) has shown that the extent of the fractured zone induced by mining in the Donetsk coal basin can be determined based on the change in natural methane emissions from this zone. After modifying the test system, he was able to locate the individual fractures at bedding-plane separations and to determine their apertures (Palchik, 2005, 2010). Further, the presence and absence of estimated horizontal fractures was correlated with uniaxial compressive strength and thickness of rock layers, distances from the extracted coal seam to the rock layer interfaces, and the thicknesses of extracted coal seams.

In addition, observations on the presence and absence of horizontal fractures at different rock layer interfaces of the overburden showed that the probability of separation increased with increasing compressive strength difference of neighboring rock layers, and with decreasing distance of the layer from the mined coal bed (Palchik, 2005; Karacan and Goodman, 2009). Therefore, bedding-plane separations and resultant strata displacements are functions of both distance from the coal seam and the type of the overlying formations. The data suggest that subsidence observed at the surface can be considered as a lumped parameter that results from the interactions of these factors. In the absence of specific data regarding the type and strength of overlying formations and their respective depths, the average value of strata displacements or average subsidence can be used as a lumped parameter with inherent uncertainty.

In this study, combined displacement profiles were constructed, and the magnitudes of strata separations in the profiles were used to generate a function for the likelihoods of strata separations and depths. The profiles were constructed from measurements of all ventholes reported in Mazza and Mlinar (1977). The data were measured using Cobalt-60 tagged shaped charges as formation markers and gamma-ray logging. This system was used in the ventholes to implant radioactive markers into the formations to measure the subsidence and the strata separation during mining, and the data are displayed in Fig. 4.

Fig. 4 shows that vertical displacements due to strata separations can occur as much as 300–350 ft above the mined coal seam (in this case, the Pittsburgh coal seam). The magnitudes of strata separations at this distance to almost 200–250 ft above of the Pittsburgh seam are generally less than 1 ft, and mostly around 0.5 ft. The displacement trend in this interval is almost linear and not a function of depth. At about 200 ft above the Pittsburgh coal bed, the separations start to depart from low displacement values, and major strata separations on the order of 2 ft can be measured. These high separations are mostly 100 ft above the coal seam, where the Sewickley sandstone occurs. This observation and the displacement measurements are in line with

the flow entry measurements discussed in the previous section. The displacement trend at and below 200 ft is nearly linear with an approximate 45-degree relationship with depth.

In order to establish a correlation between strata displacement (SD) and depth, an exponential function was fitted to field measurements (Fig. 4). This function was later used as a surrogate to approximate surface subsidence, in accordance with treating average subsidence as a lumped parameter. Representative average strata displacement, used as a surrogate for subsidence, was calculated as the sum of the displacements at depth intervals where the bottom and top of the slotted casing were located with respect to the top of coal bed. This relation is given as:

$$\boldsymbol{SD} = \left( -\frac{\ln\left(\frac{\boldsymbol{D}_1}{350}\right)}{0.698} \right) + \left( -\frac{\ln\left(\frac{\boldsymbol{OB}-\boldsymbol{D}_2}{350}\right)}{0.698} \right) \quad (4)$$

where $D_1$ is the distance from bottom of slotted casing to top of coal bed, $D_2$ distance from surface to the top of slotted casing, and OB is the overburden depth. Vertical and horizontal anisotropies are not considered independently, but are simply part of the lumped parameter.

*2.3.3. Gas content of overlying formations (coal beds)*

Determining the source of longwall methane and of the gas produced from gob gas ventholes is important since the gas source may dictate the amount and composition of the gas. Diamond et al. (1992) conducted a series of field tests in the Lower Kittanning coal bed. Boreholes were drilled before and after mining a panel, in order to obtain coal and rock samples from overlying strata, and to determine their gas contents. The modified direct method (MDM) was employed to determine the gas contents of recovered coal and rock samples (Diamond and Schatzel, 1998). The results indicated that approximately 90% of the gas removed from the overlying strata came from coal beds. Material balance calculations were made to compare the volume of gas produced from GGVs drilled over the panel and gas removed by the mine's ventilation system with the volume of gas removed from strata directly overlying the panel to a height of 275 ft.

Since most longwall gas comes from overlying coal beds, the gas contents of the coals in the Pennsylvania (PA) section of the Northern Appalachian basin were compiled from Diamond et al. (1986) and plotted versus depth as shown in Fig. 5. This plot established a relation between gas content and depth, and was incorporated into the deterministic equations as an input parameter affecting gas rate and methane concentration from the GGVs. Here, the relation was represented with a linear trend of gas content increase with increasing depth.

Almost all the coals that are reported in Diamond et al. (1986) for PA are high volatile bitumious A, with lesser amounts of B and C, but this is not true in all coal basins. In order to include the gas contents of coals of all ranks into the predictive equations, all HV (A, B and C), medium- and low-rank coals, and sub-bituminous (A, B and C) coals from all basins that are reported in Diamond et al. (1986) were compiled and grouped into 3 main classes of rank and gas content (HV, MV–LV, and sub-bituminous), as distributions. This compilation is found in Section 3, Table 4.

*2.3.4. Modified deterministic equations for gas production rate and methane concentration prediction from gob gas ventholes*

In order to modify the original deterministic equations and their parameter coefficients, the parameters discussed in the previous sections were added to original equations as linear combinations. Since distance to the top of the slotted casing and casing length are related and create multi-colinearity, only distance to the top of the slotted casing was included in the new equations. Casing length can easily be calculated with knowledge of overburden depth, distance to top of slotted casing, and the distance from bottom of slotted casing to top of coal bed.

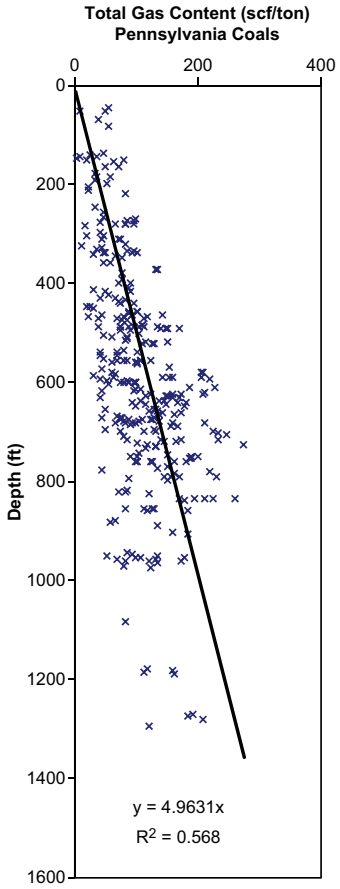


**Fig. 5.** Total gas contents of high volatile bituminous (HV) coal beds of Pennsylvania and their variations with overburden depth.

The modified equations, shown as Eqs. (5) and (6), representing well production rates and methane concentration, respectively, were fitted to the same production flow rate and methane concentration data obtained earlier from the MCP software, for both A-A and C-I cases.

$$\text{GGV Production Rate (scfm)} = P_1 \times x_1 + P_2 \times x_2 + \ldots\ldots + P_n \times x_n \quad (5)$$

$$\text{Methane (\%)} = R_1 \times y_1 + R_2 \times y_2 + \ldots\ldots + R_n \times y_n \quad (6)$$

These equations, when fitted to the gas production rate and methane concentration data, resulted in regression coefficients ($R^2$) of 0.83 and 0.69 for prediction of production rate from A-A and C-I cases, respectively. For prediction of methane concentrations, the regression coefficients were 0.89 and 0.74 for A-A and C-I cases, respectively. These values are very close to the ones obtained by using Eqs. (1) and (2), shown in Table 1.

Table 2 gives the new coefficients of input parameters for Eqs. (5) and (6), with the extra parameters from the modified equations in bold. Analysis of parameter coefficients shows neither distance to top of slotted casing (and thus slotted casing length) nor subsidence produce statistically significant effects on methane concentration in either A-A or C-I cases. Gas content of the coal bed had no statistically significant effects on production flow rate of GGVs.

**Table 2**
Parameters and coefficients of the modified multilinear regression equations that were developed for calculating production rates and methane concentrations from GGVs for A-A and C-I cases.

| Production rate (scfm) — Case: A-A | | | | Methane concentration (%) — Case: A-A | | | |
|---|---|---|---|---|---|---|---|
| Parameter | | Coefficient | | Parameter | | Coefficient | |
| Intercept | | 0.000E + 00 | | Intercept | | 0.000E + 00 | |
| Distance to top of slotted casing (ft) Face past BH | $P_1$ | 1.277E + 00 | $x_1$ | Distance to top of slotted casing (ft) Face past BH | $R_1$ | 0.000E + 00 | $y_1$ |
| Location (ft) | $P_2$ | −2.051E−02 | $x_2$ | Location (ft | $R_2$ | 3.334E−04 | $y_2$ |
| Linear adv. rate (ft/day) | $P_3$ | 4.926E−01 | $x_3$ | Linear adv. rate (ft/day) | $R_3$ | 1.254E−01 | $y_3$ |
| Surface elevation (ft) | $P_4$ | −2.301E−01 | $x_4$ | Surface elevation (ft) | $R_4$ | −1.468E−02 | $y_4$ |
| Average OB depth (ft) | $P_5$ | −1.084E + 00 | $x_5$ | Average OB depth (ft) | $R_5$ | 5.416E−02 | $y_5$ |
| Casing diameter (″) | $P_6$ | 1.549E + 02 | $x_6$ | Casing diameter (″) | $R_6$ | −9.379E + 00 | $y_6$ |
| Slotted Casing height from top of coal (ft) | $P_7$ | −1.112E + 01 | $x_7$ | Slotted Casing height from top of coal (ft) | $R_7$ | 4.509E−02 | $y_7$ |
| Distance to TG (ft) | $P_8$ | −9.449E−01 | $x_8$ | Distance to TG (ft) | $R_8$ | −2.068E−01 | $y_8$ |
| Distance from start (ft) | $P_9$ | 5.538E−03 | $x_9$ | Distance from start (ft) | $R_9$ | −1.226E−03 | $y_9$ |
| Panel length (ft) | $P_{10}$ | 2.567E−02 | $x_{10}$ | Panel Length (ft) | $R_{10}$ | 3.484E−02 | $y_{10}$ |
| Panel width (ft) | $P_{11}$ | 3.579E−01 | $x_{11}$ | Panel width (ft) | $R_{11}$ | −1.276E−01 | $y_{11}$ |
| Atm. press (in Hg) | $P_{12}$ | 1.574E + 01 | $x_{12}$ | Atm. press (in Hg) | $R_{12}$ | −2.307E + 00 | $y_{12}$ |
| Ext vacuum (in water) | $P_{13}$ | −1.611E + 00 | $x_{13}$ | Ext vacuum (in water) | $R_{13}$ | −3.847E−02 | $y_{13}$ |
| Coal gas content (scf/ton) | $P_{14}$ | 0.000E + 00 | $x_{14}$ | Coal gas content (scf/ton) | $R_{14}$ | 3.526E−02 | $y_{14}$ |
| Subsidence (ft) | $P_{15}$ | −2.493E + 02 | $x_{15}$ | Subsidence (ft) | $R_{15}$ | 0.000E + 00 | $y_{15}$ |
| $R^2 = 0.83$ | | | | $R^2 = 0.89$ | | | |

| Production rate (scfm) — Case: C-I | | | | Methane concentration (%) — Case: C-I | | | |
|---|---|---|---|---|---|---|---|
| Parameter | | Coefficient | | Parameter | | Coefficient | |
| Intercept | | 0.000E + 00 | | Intercept | | 0.000E + 00 | |
| Distance to top of slotted casing (ft) | $P_1$ | 6.463E + 00 | $x_1$ | Distance to top of slotted casing (ft) | $R_1$ | 0.000E + 00 | $y_1$ |
| Surface elevation (ft) | $P_2$ | 2.734E−02 | $x_2$ | Surface elevation (ft) | $R_2$ | 9.734E−03 | $y_2$ |
| Average OB depth (ft) | $P_3$ | −6.222E + 00 | $x_3$ | Average OB depth (ft) | $R_3$ | −1.194E−02 | $y_3$ |
| Casing diameter (″) | $P_4$ | 5.477E + 01 | $x_4$ | Casing diameter (″) | $R_4$ | 1.642E−01 | $y_4$ |
| Slotted casing height from top of Coal (ft) | $P_5$ | 1.594E + 01 | $x_5$ | Slotted casing height from top of Coal (ft) | $R_5$ | −1.242E + 00 | $y_5$ |
| Distance to TG (ft) | $P_6$ | −2.245E−01 | $x_6$ | Distance to TG (ft) | $R_6$ | −4.917E−02 | $y_6$ |
| Distance from start (ft) | $P_7$ | −3.187E−03 | $x_7$ | Distance from start (ft) | $R_7$ | 9.722E−04 | $y_7$ |
| Panel length (ft) | $P_8$ | 4.136E−03 | $x_8$ | Panel length (ft) | $R_8$ | 6.985E−03 | $y_8$ |
| Panel width (ft) | $P_9$ | −2.769E−01 | $x_9$ | Panel width (ft) | $R_9$ | −2.234E−02 | $y_9$ |
| Atm. press (in Hg) | $P_{10}$ | 7.302E + 00 | $x_{10}$ | Atm. press (in Hg) | $R_{10}$ | 2.513E + 00 | $y_{10}$ |
| Ext vacuum (in water) | $P_{11}$ | −3.670E + 00 | $x_{11}$ | Ext vacuum (in water) | $R_{11}$ | −1.066E−01 | $y_{11}$ |
| Coal gas content (scf/ton) | $P_{12}$ | 0.000E + 00 | $x_{12}$ | Coal gas content (scf/ton) | $R_{12}$ | 1.430E−02 | $y_{12}$ |
| Subsidence (ft) | $P_{13}$ | 1.380E + 02 | $x_{13}$ | Subsidence (ft) | $R_{13}$ | 0.000E + 00 | $y_{13}$ |
| $R^2 = 0.69$ | | | | $R^2 = 0.74$ | | | |

The results obtained using the original deterministic equations (Table 1) and the modified equations (Table 2) were also compared using values of descriptive statistics obtained from the predictions of production rate and methane concentration. These data are given in Table 3. Almost all descriptive values are very similar for predictions of rates and methane percentages. In both A-A and C-I cases, absolute value of the skewness decreased, indicating a more normal distribution of results with the modified models.

## 3. Stochastic method for evaluating production rates and methane concentrations using distributions of input parameters

### *3.1. Generating probability density functions (PDF) for distribution of input values*

To move from a deterministic model to a stochastic model, probability distributions over the range of values for each parameter must be determined. Monte Carlo simulation generates random values for input parameters in a model whose parameters cannot be defined by exact functions, but by probability density functions (PDFs). Describing the population of any variable using probability density functions is helpful when direct integration of the function of that variable in a model is not practical or when the exact behavior of that variable is not known. The PDFs that best describe these populations can then be used to generate random values for each variable to be used in deterministic models. Once the likely probability density function has been determined, a random number is fed into the inverse equation to determine the value to be generated for the distribution of any input parameter. The

**Table 3**
Descriptive statistics for the rate and methane concentration outputs obtained by two sets of equations.

| A-A case (active panel; advancing face) | Original multilinear eq. (Eqs. (1) and (2)) | Modified multilinear eq. (Eqs. (5) and (6)) |
|---|---|---|
| Rate (mean) | 224.91 | 210.94 |
| Rate (std. dev.) | 189.98 | 157.42 |
| Rate (median) | 224.72 | 209.87 |
| Rate (variance) | 36094.22 | 24783.70 |
| Rate (skewness) | 0.140 | -0.010 |
| Methane % (mean) | 57.04 | 56.18 |
| Methane % (std. dev.) | 27.29 | 27.29 |
| Methane % (median) | 57.29 | 56.52 |
| Methane % (variance) | 745.25 | 744.96 |
| Methane % (skewness) | -0.021 | -0.021 |
| **C-I case (completed panel; idle face)** | **Original multilinear eq. (Eqs. (1) and (2))** | **Modified multilinear eq. (Eqs. (5) and (6))** |
| Rate (mean) | 183.19 | 187.61 |
| Rate (std. dev.) | 78.24 | 81.81 |
| Rate (median) | 186.02 | 189.38 |
| Rate (variance) | 6122.67 | 6694.48 |
| Rate (skewness) | -0.039 | 0.00007 |
| Methane % (mean) | 57.25 | 56.91 |
| Methane % (std. dev.) | 11.92 | 11.94 |
| Methane % (median) | 57.08 | 56.73 |
| Methane % (variance) | 142.23 | 142.66 |
| Methane % (skewness) | 0.017 | 0.016 |

random number is generated from a uniform distribution between 0 and 1, so that it falls in an unbiased percentile range. The inversion is employed in the sampling method stage (Ripley, 1987; Vose, 2000).

The output of a deterministic model that is solved this way is reasonably accurate only if the number of simulations is very large. The advantage of this method is that the complete probability distribution of the model output can be obtained (Sari, 2009).

In this section, the distributions of input data used in the MCP software for production rate and methane concentration for A-A and C-I cases are used to make generalizations about the populations of each of the input parameters. These generalizations are then used in Monte Carlo simulations of the modified deterministic equations (Eqs. (5) and (6)) for estimating and generalizing production rate and methane percentages in A-A and C-I cases.

Fig. 6A–F shows example input variables "GGV distance from panel start", "casing diameter", and "extraction vacuum" and their distributions for the A-A and C-I cases, used in generating rate and methane percentage outputs from MCP. As mentioned in Section 2.3.3, gas

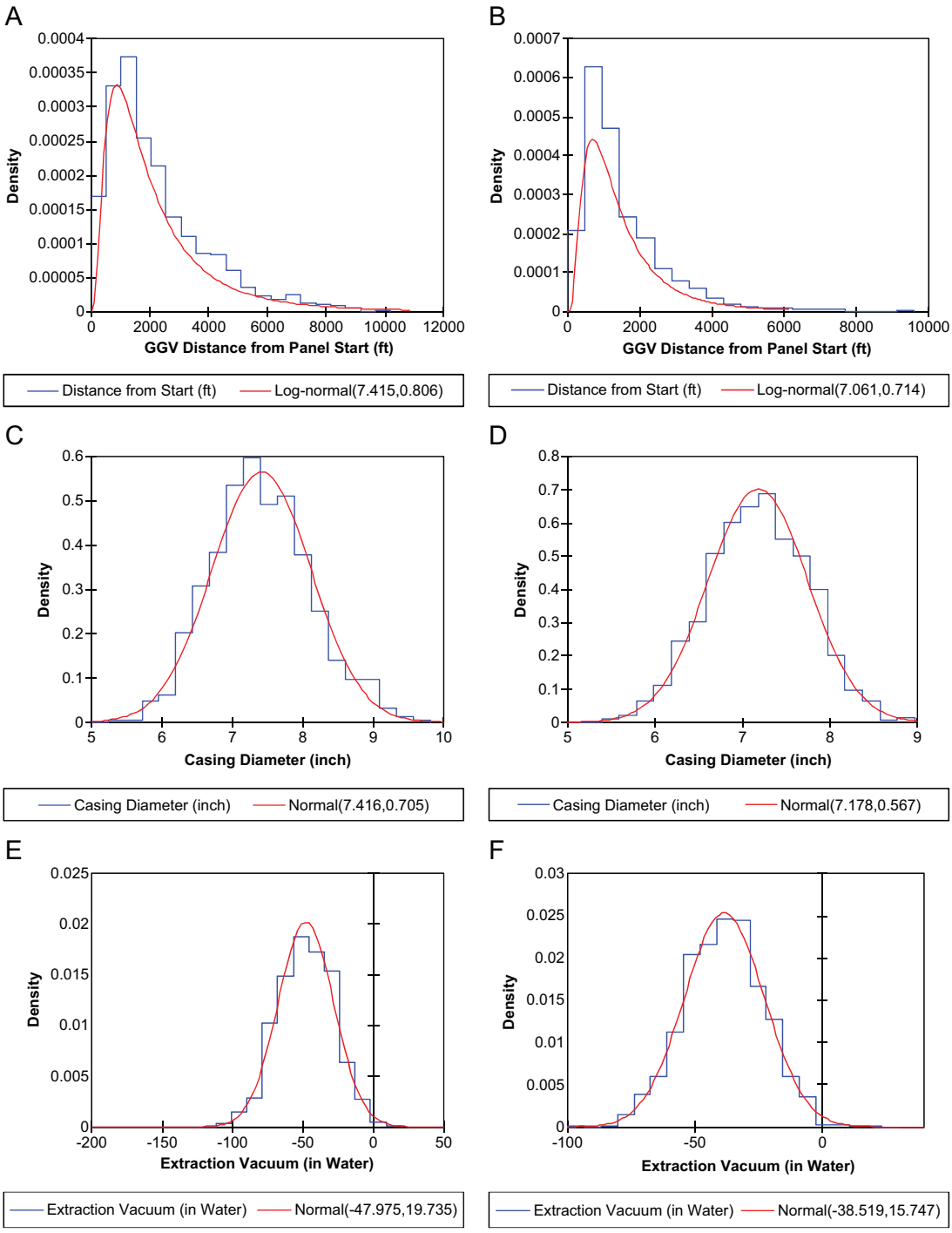


**Fig. 6.** Example PDFs for the values used in running MCP for rate and methane percentage estimations from GGVs in A-A (A, C, and E) and C-I (B, D, and F) cases.

contents of coals of HV (high volatile), MV (medium volatile) and LV (low volatile), and sub-bitiminous ranks were included in the predictive equations of the A-A and C-I cases as 3 main classes (Table 4).

In order to generalize the populations of input values, they were compared against different distribution functions, as shown in Fig. 6 for the example inputs, and as given in Table 7 for all input variables of the modified equations. Densities of the values for each of the inputs were statistically compared to the hypothetical distributions to ensure that the "assumption" of a selected distribution would represent the data distribution. This statistical procedure is called the goodness-of-fit test.

For the goodness-of-fit test described above, the Kolmogorov–Smirnov (K–S) test (Chakravarti et al., 1967) was used. The K–S test is based on:

$$\boldsymbol{D} = \max_{1 \le i \le N} \left( \boldsymbol{F}(\boldsymbol{Y}_i) - \frac{\boldsymbol{i}-1}{\boldsymbol{N}}, \frac{\boldsymbol{i}}{\boldsymbol{N}} - \boldsymbol{F}(\boldsymbol{Y}_i) \right) \tag{7}$$

In this equation, $Y_i$ are the data pairs ordered from smallest to largest value ($Y_1$, $Y_2$… $Y_N$). N is the number of ordered data pairs. F is the theoretical cumulative distribution of the sample distribution being tested and it must be fully specified with mean and standard deviation. The test starts with a hypothesis that the data follow a specified distribution ($H_0$) and a significance level ($\alpha$). The hypothesis regarding the proposed distribution is rejected if the test statistic, D, is greater than the critical value, p, obtained for the corresponding significance level, and if the critical value p is less than the significance level. In that case, the use of an alternative distribution is suggested ($H_a$). If a hypothesis is accepted, the value of p is the risk of rejecting that hypothesis although it is true.

In this work, 0.01 was used as significance level in all the tests and for all variables, from which the K–S statistics and critical values given in Table 4 were obtained. Table 4 shows that distributions of most values can be represented either by normal (N) or log-normal (LN) distributions with specified means ($\mu$) and standard deviations ($\sigma$). The density functions for normal and log-normal distributions are given in Eqs. (8) and (9), respectively.

$$\boldsymbol{f}(\boldsymbol{x}) = \frac{1}{\boldsymbol{\sigma}\sqrt{2\boldsymbol{\pi}}} \boldsymbol{e}^{\frac{(x-\mu)^2}{2\sigma^2}}; \quad \boldsymbol{\sigma} > 0 \tag{8}$$

$$\boldsymbol{f}(\boldsymbol{x}) = \frac{1}{\boldsymbol{x}\boldsymbol{\sigma}\sqrt{2\boldsymbol{\pi}}} \boldsymbol{e}^{\frac{(\ln(x)-\mu)^2}{2\sigma^2}}; \quad \boldsymbol{x}, \boldsymbol{\sigma} > 0 \tag{9}$$

### 3.2. Monte Carlo (MC) simulations

RiskAMP™ (Structured Data, 2008) was used as the Monte Carlo simulator in this work. This program provides utilization of Monte Carlo functions and random distributions as MS-Excel™ add-in features and creates spreadsheet models that employ Monte Carlo simulations.

In this study, 5000 simulations for each of the coal ranks (HV, MV–LV and sub-bituminous) in each of the longwall cases (A-A and C-I) in Table 4 were run using the Latin Hypercube sampling technique. Latin

**Table 4**
Generalized distributions, and their means and standard deviations, obtained for each of the input variables and the results of K–S statistics for hypothesis testing for goodness-of-fit.

A-A case: (active panel; advancing face)

| Parameter | Distribution ($\mu$, $\sigma$) | Kolmogorov–Smirnov test (D; p) |
|---|---|---|
| Distance to SC top (ft) | N (502.982; 85.069) | (0.018; 0.905) |
| Face past BH location (ft) | N (3182.644; 1783.761) | (0.039; 0.103) |
| Linear adv. rate (ft/day) | N (30.123; 14.250) | (0.022; 0.724) |
| Surface elevation (ft) | N (1252.033; 111.941) | (0.025; 0.596) |
| Average OB depth (ft) | N (749.435; 67.908) | (0.019; 0.884) |
| Casing diameter (″) | N (7.416; 0.705) | (0.026; 0.531) |
| Slotted casing height from top of coal (ft) | N (43.395; 6.34) | (0.013; 0.996) |
| Distance to TG (ft) | N (277.419; 27.191) | (0.017; 0.942) |
| Distance from start (ft) | LN (7.415; 0.806) | (0.032; 0.283) |
| Panel length (ft) | N (10702.566; 548.847) | (0.018; 0.921) |
| Panel width (ft) | N (1282.733; 62.508) | (0.024; 0.629) |
| Atm. press (in Hg) | N (26.071; 2.922) | (0.025; 0.610) |
| Ext vacuum (in water) | N (−49.975; 19.735) | (0.024; 0.634) |
| Subsidence (ft) | N (3.585; 0.395) | (0.047; 0.331) |

C-I case: (completed panel; idle face)

| Parameter | Distribution ($\mu$, $\sigma$) | Kolmogorov–Smirnov test (D; p) |
|---|---|---|
| Distance to SC top (ft) | N (522.514; 68.786) | (0.023; 0.690) |
| Surface elevation (ft) | N (1176.299; 99.239) | (0.026; 0.486) |
| Average OB depth (ft) | N (741.300; 59.929) | (0.022; 0.706) |
| Casing diameter (″) | N (7.178; 0.567) | (0.020; 0.831) |
| Slotted casing height from top of coal (ft) | N (44.522; 7.242) | (0.015; 0.979) |
| Distance to TG (ft) | N (266.941; 41.001) | (0.024; 0.605) |
| Distance from start (ft) | LN (7.061; 0.714) | (0.023; 0.687) |
| Panel length (ft) | N (10350.710; 692.338) | (0.023; 0.660) |
| Panel width (ft) | N (1249.957; 103.286) | (0.028; 0.423) |
| Atm. press (in Hg) | N (27.376; 1.776) | (0.023; 0.681) |
| Ext vacuum (in water) | N (−38.519; 15.747) | (0.017; 0.944) |
| Subsidence (ft) | N (3.715; 0.392) | (0.037; 0.127) |

| Coal rank–gas content (scf/ton) | | Distribution ($\mu$, $\sigma$) | Kolmogorov–Smirnov test (D; p) |
|---|---|---|---|
| High vol. bit. (A, B, and C) coals | **A-A** | LN (4.270; 1.078) | (0.043; 0.630) |
| Low–medium volatile coals | | N (356.957; 136.895) | (0.041; 0.660) |
| Sub-bit. (A, B, and C) coals | | LN (1.906; 0.918) | (0.038; 0.703) |
| High vol. bit. (A, B, and C) coals | **C-I** | LN (4.270; 1.083) | (0.053; 0.314) |
| Low–medium volatile coals | | N (364.496; 134.395) | (0.024; 0.989) |
| Sub-bit. (A, B, and C) coals | | LN (1.794; 0.853) | (0.026; 0.975) |

Hypercube sampling is a sampling method usually utilized for close representation of the parameter probability distributions and was first described by McKay et al (1979) as an appropriate method for selecting values of input parameters. These cases were run using the generalized distributions given for each input in Table 4 in modified linear regression equations, Eqs. (5) and (6), as predictors for the GGV performance parameters.

It should be noted that Monte Carlo simulation cannot easily include the covariance between input variables, resulting in shortcomings as far as joint uncertainty of input variables is concerned. This problem is usually solved with Bayesian Markov Chain Monte Carlo methods (Ades and Lu, 2003). However, this discussion is beyond the scope of this paper.

### *3.2.1. Conditional arguments to MC simulations for refinement of parameter ranges*

Problems with unrealistic input values or unacceptable calculated outputs can arise in random simulations. This usually occurs when sampling values from either side of the distributions, and is due to the departure of representative distribution functions from the actual data. In order to correct this problem, a set of conditional arguments can be defined.

Five thousand MC simulations were executed for each of the three coal ranks, and each of the two longwall cases to produce 30,000 ($6\times5000$) different possible combinations of production rate and methane percentage outputs, each of which corresponded to a certain combination of random inputs. Conditional arguments were used to correct for unrealistic inputs and outputs.

The generated input data was run through a series of IF THEN routines to control the validity of the input values. Input values that violated the conditions would result in the entire row of inputs being assigned null values. For example, any distance, depth, or gas content value must be positive. So, if the value generated for the "distance to the top of slotted casing" was negative, then those sets of inputs were assigned null values. Similarly, the routines checked for impossible combinations of values. For example, if the sum of the values generated for "face past borehole location" and "distance of borehole from panel start" was greater than the value generated for "panel length," then those inputs were assigned null values.

Another set of IF THEN statements was implemented for the generated output values. Production rates and methane percentages cannot be negative, and methane percentage cannot be lower than 10% (as an operational constraint) and cannot exceed 100%. Any combinations of input values that gave outputs that violated these conditions were also assigned null values and eventually removed from input–output data.

Imposing conditions on inputs and outputs during MC simulations results in defining the ranges of input values that gave reasonable outputs. Once the populations and ranges of these input values were defined, minimum, mean and maximum values for the ranges could be determined. These values are given in Table 5.

**Table 5**
Value ranges that are generated as a result of conditional MC to use in modified equations.

| A-A case: (active panel; advancing face) | | |
|---|---|---|
| Parameter | | Min; mean; max |
| Distance to SC top (ft) | | (201.9; 502.9; 790.1) |
| Face past BH location (ft) | | (9.4; 3182.6; 9128.3) |
| Linear adv. rate (ft/day) | | (0.1; 30.1; 107.4) |
| Surface elevation (ft) | | (918.3; 1232.0; 1573.8) |
| Average OB depth (ft) | | 510.1; 743.4; 988.2) |
| Casing diameter (″) | | (5.3; 7.4; 9.7) |
| Slotted casing height from top of coal (ft) | | (24.0; 43.4; 64.1) |
| Distance to TG (ft) | | (204.3; 277.4; 379.2) |
| Distance from start (ft) | | (144.9; 2230.6; 10138.5) |
| Panel length (ft) | | (9010.6; 10702.6; 12215.5) |
| Panel width (ft) | | (1099.2; 1282.7; 1448.5) |
| Atm. press (in Hg) | | (16.6; 26.1; 34.7) |
| Ext vacuum (in water) | | (−110.5; −47.9; 17.8) |
| Overlying coal gas content | HV bit. | (1.8; 118.5; 699.6) |
| (scf/ton) | LV–MV bit. | (29.4; 356.9; 715.7) |
| | Sub-bit. | (0.7; 10.4; 135.9) |
| Subsidence (ft) | | (2.6; 3.6; 5.1) |
| C-I case: (completed panel; idle face) | | |
| Parameter | | Min; mean; max |
| Distance to SC top (ft) | | (254.7; 522.5; 739.4) |
| Surface elevation (ft) | | (884.5; 1176.3; 1527.9) |
| Average OB depth (ft) | | (515.4; 741.3; 937.6) |
| Casing diameter (″) | | (5.4; 7.2; 8.9) |
| Slotted casing height from top of coal (ft) | | (20.1; 44.5; 65.8) |
| Distance to TG (ft) | | (123.4; 266.9; 399.4) |
| Distance from start (ft) | | (153.6; 1503.7; 9526.7) |
| Panel length (ft) | | (8301.3; 10350.7; 12830.5) |
| Panel width (ft) | | (926.5; 1249.9; 1599.6) |
| Atm. press (in Hg) | | (21.1; 27.4; 33.5) |
| Ext vacuum (in Water) | | (-99.1; -38.5; 22.2) |
| Overlying coal gas content | HV bit. | (2.2; 115.2; 676.4) |
| (scf/ton) | LV–MV bit. | (13.5; 364.5; 707.7) |
| | Sub-bit. | (0.8; 8.7; 69.7) |
| Subsidence (ft) | | (2.7; 3.7; 5.3) |

## 4. Results: production rate and methane concentration distributions

Conditional arguments imposed during MC simulations resulted in ranges of input values that could be applicable to modeling GGV productions (Table 5) and methane concentrations. Probability density functions of rate and methane concentration distributions computed using MC simulations within the range of values given in Table 5 are given in Figs. 7 and 8 for A-A and C-I cases, respectively. Figs. 7 and 8 also show that rate and methane concentration outputs can be represented with normal distributions with varying mean and standard deviation values depending on the rank of coals in overlying formations.

Fig. 7 shows that, for a GGV operating in an A-A situation with the overlying formation containing HV coals, the most probable GGV production rate is 200–250 scfm (Fig. 7-A), although the rate can be as high as 650 scfm. With different combinations of input values, the most likely methane concentration is 55–60%. Concentrations can be as high as 100% in the produced gas (Fig. 7-D).

Fig. 7-B, E, C and F shows the resultant distributions of rate and methane concentration with medium–low volatile coals and subbituminous coals in the overburden, respectively. These distributions show that medium-low volatile coals in the overburden most likely produce 240 scfm (B) at a concentration of 40–80% (E). Subbituminous coals in the overburden, on the other hand, can result in a most probable rate of 230 scfm (C) and a most probable methane concentration around 50% (F).

Fig. 8 shows the possible values of production rate and methane percentage that might be expected from a GGV operating in a completed longwall panel. The figure shows that higher rates, in general, can be achieved with different combinations of input values compared to the A-A shown in Fig. 7. Since methane concentrations generally tend towards lower values and the maximum methane concentrations are at most 90%, this data may suggest that higher rates are due to drawing more air, instead of methane, into the GGV for a given combination of location, drilling, and operation parameters.

Table 6 shows the descriptive statistical values calculated using the distributions of rates and methane concentrations obtained from MC simulations. The values for the A-A case show that mean production rates and methane concentrations are slightly higher in the case of medium-low volatile coals present in overlying gas formations.

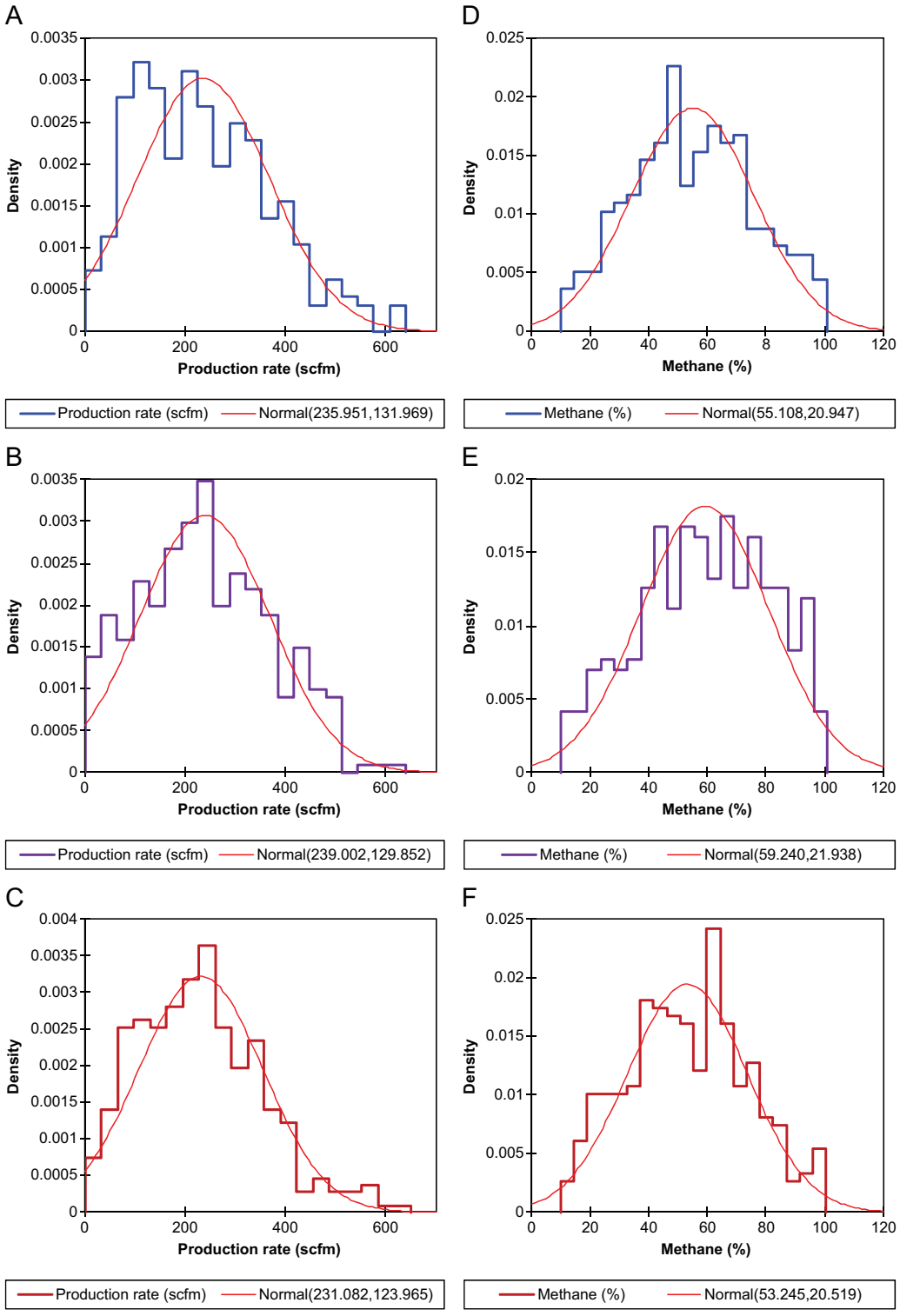


**Fig. 7.** PDFs of rate (A, B, and C) and methane percentage (D, E, and F) outputs obtained from conditional MC simulations for A-A case, for HV coals (A and D), MV–LV coals (B and E), and sub-bituminous coals (C and F), and the normal distributions fitted to those.

Predicted maximum rates are around 640 scfm with methane concentrations as high as 100% in all cases. The C-I values show that rates in that case have mean values of 330–340 scfm, with extreme values of 750–800 sfcm. Maximum methane concentrations for the C-I case do not exceed 90%.

A more efficient way of interpreting the results of an MC simulation is to analyze the calculated percentiles. Fig. 9 shows the percentiles corresponding to the different production rate (A) and methane percentage outputs (B) from conditional MC simulations. These results show that it is more probable for a GGV to produce at

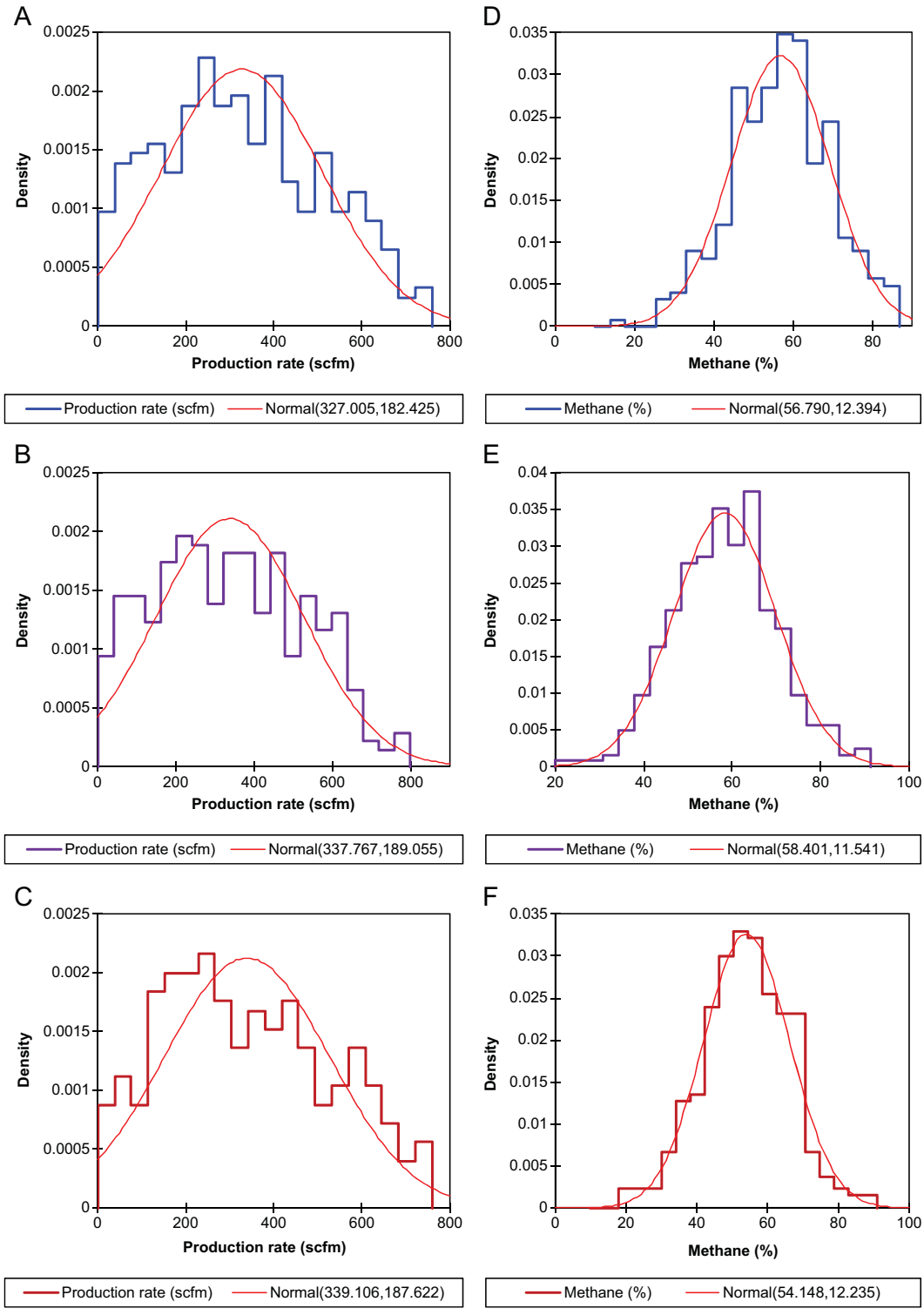


**Fig. 8.** PDFs of rate (A, B, and C) and methane percentage (D, E, and F) outputs obtained from conditional MC simulations for C-I case, for HV coals (A and D), MV–LV coals (B and E), and sub-bituminous coals (C and F). Also shown are the fitted normal distributions.

higher rates in a C-I situation than in an A-A situation. However, the probability of producing higher methane concentrations is greater in an A-A situation. Further, in the C-I case, a large range of GGV production percentiles (20th–70th) is windowed in a narrow methane concentration (50–60%) range, indicating a relatively high probability of producing gas within this methane percentage range. This suggests that changes in input parameter values have a relatively small effect on methane concentration for C-I cases.

The results shown in Fig. 9 are presented in Table 7 in tabulated form. In this table, the rates and methane concentrations

**Table 6**
Summary of descriptive statistics performed on the MC results.

| A-A case: (active panel; advancing face) | | | | | | |
|---|---|---|---|---|---|---|
| | HV coals | | MV-LV coals | | Sub-bit. coals | |
| Parameter | Rate (scfm) | Methane (%) | Rate (scfm) | Methane (%) | Rate (scfm) | Methane (%) |
| Mean | 235.95 | 55.11 | 239.00 | 59.24 | 231.08 | 53.24 |
| Standard deviation | 131.97 | 20.95 | 129.85 | 21.93 | 123.96 | 20.52 |
| Skewness | 0.57 | 0.07 | 0.27 | -0.18 | 0.59 | 0.09 |
| Minimum | 12.33 | 10.33 | 10.28 | 10.68 | 10.34 | 11.51 |
| Maximum | 638.92 | 99.69 | 632.01 | 100.00 | 644.47 | 99.51 |
| C-I case: (completed panel; idle face) | | | | | | |
| | HV coals | | MV–LV coals | | Sub-bit. coals | |
| Parameter | Rate (scfm) | Methane (%) | Rate (scfm) | Methane (%) | Rate (scfm) | Methane (%) |
| Mean | 327.00 | 56.79 | 337.76 | 58.40 | 339.11 | 54.15 |
| Standard deviation | 182.42 | 12.39 | 189.05 | 11.54 | 187.62 | 12.23 |
| Skewness | 0.25 | -0.11 | 0.20 | 0.01 | 0.27 | -0.09 |
| Minimum | 10.79 | 15.84 | 10.29 | 21.63 | 11.26 | 18.88 |
| Maximum | 752.27 | 85.59 | 799.73 | 90.27 | 753.13 | 90.18 |

corresponding to 20th, 50th and 80th percentiles are shown in red to highlight values which exhibit low-, mean- and high-possibilities for the total number of iterations. For the A-A case, 80% of total iterations resulted in production rates of 350 scfm or lower and methane concentrations of 73% or lower when there were HV coals in the fractured overburden. The numbers for the same percentile for the C-I case and HV coals in the overlying strata as the main methane source

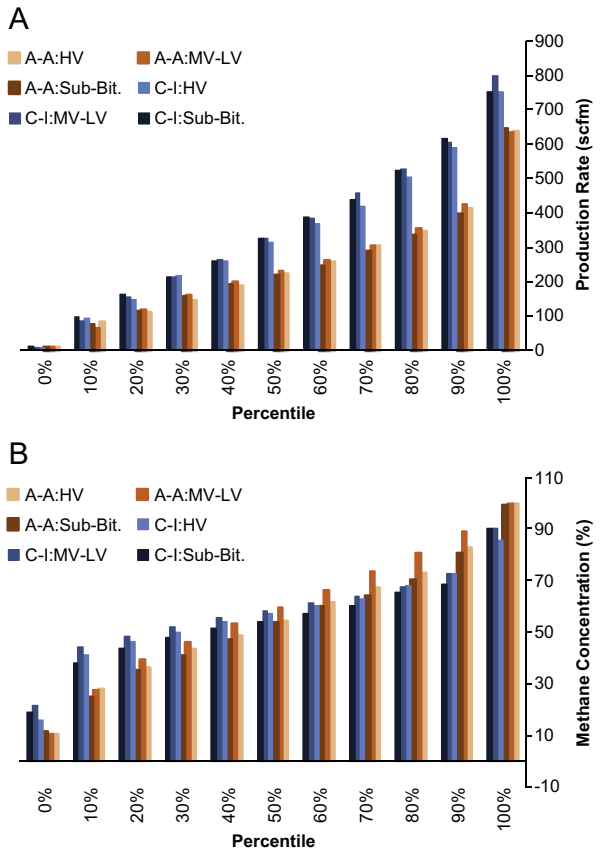


**Fig. 9.** Percentiles corresponding to different production rate (A) and methane percentage outputs (B) from conditional MC simulations.

**Table 7**
Tabulated percentiles of the data presented in Fig. 9.

| A-A case: (active panel; advancing face) | | | | | | |
|---|---|---|---|---|---|---|
| Coal rank | HV bit. coals | | MV–LV coals | | Sub-bit. coals | |
| Percentile | Prod. rate (scfm) | Methane (%) | Prod. rate (scfm) | Methane (%) | Prod. rate (scfm) | Methane (%) |
| 100% | 638.93 | 99.7 | 632.02 | 100.0 | 644.47 | 99.5 |
| 90% | 412.83 | 83.0 | 423.64 | 89.2 | 396.45 | 80.6 |
| **80%** | **349.24** | **72.8** | **356.71** | **80.7** | **337.02** | **70.5** |
| 70% | 304.92 | 67.4 | 306.35 | 73.6 | 287.97 | 64.4 |
| 60% | 258.08 | 61.5 | 264.17 | 66.5 | 247.27 | 60.2 |
| **50%** | **222.12** | **54.5** | **230.37** | **59.5** | **220.25** | **53.7** |
| 40% | 187.89 | 48.9 | 200.85 | 53.3 | 194.37 | 47.0 |
| 30% | 146.89 | 43.8 | 163.69 | 46.2 | 159.21 | 40.8 |
| **20%** | **112.62** | **36.2** | **118.27** | **39.3** | **115.13** | **35.5** |
| 10% | 84.61 | 27.9 | 63.77 | 27.7 | 76.10 | 24.9 |
| 0% | 12.33 | 10.3 | 10.29 | 10.7 | 10.35 | 11.5 |
| C-I case: (completed panel; idle Face) | | | | | | |
| Coal rank | HV bit. coals | | MV–LV coals | | Sub-bit. coals | |
| Percentile | Prod. rate (scfm) | Methane (%) | Prod. rate (scfm) | Methane (%) | Prod. rate (scfm) | Methane (%) |
| 100% | 752.27 | 85.6 | 799.73 | 90.3 | 753.13 | 90.2 |
| 90% | 588.18 | 72.7 | 603.49 | 72.7 | 617.09 | 68.7 |
| **80%** | **504.49** | **67.9** | **526.59** | **67.7** | **521.88** | **65.7** |
| 70% | 419.28 | 62.9 | 456.71 | 64.1 | 437.03 | 60.5 |
| 60% | 368.88 | 60.2 | 385.81 | 61.5 | 387.35 | 57.2 |
| **50%** | **313.42** | **57.4** | **328.16** | **58.5** | **327.82** | **54.1** |
| 40% | 261.46 | 54.3 | 264.30 | 55.7 | 259.03 | 51.5 |
| 30% | 219.31 | 50.0 | 215.96 | 52.1 | 214.21 | 48.1 |
| **20%** | **149.38** | **46.3** | **155.91** | **48.7** | **165.39** | **43.9** |
| 10% | 94.22 | 41.3 | 85.18 | 44.2 | 97.34 | 38.0 |
| 0% | 10.79 | 15.8 | 10.30 | 21.6 | 11.26 | 18.9 |

The numbers in bold correspond to 20%, 50% and 80% percentiles, which were selected as the low, mean and high values within the range.

are 504 scfm or less and 68% or less. Similarly, analyses can be conducted for other coal ranks and at different percentiles.

The ranges of GGV and mine operation parameters given in Table 5 are suitable to cover most longwall operations. The parameters most likely to fall outside these ranges may be highly location-dependent parameters such as the depths and surface elevations, and thus the length of the slotted casing. In order to evaluate the effects on predicted GGV production rates and methane concentrations in situations where distance to slotted casing top, surface elevation, and overburden depths are larger than given in Table 5, the allowable ranges of these parameters were raised, following normal distributions. This gave the minimum, mean and maximum values tabulated in Table 8 for A-A and C-I conditions. Changing only these parameters, while keeping the others constant, increases the length of the slotted casing.

MC simulations were performed with the data given in Table 8 for A-A and C-I cases, keeping the values of the other parameters as in Table 5. Simulation results are shown as percentiles in Fig. 10-A and B

**Table 8**
Parameters and their value ranges that are changed to evaluate responses of production rate and methane concentration from a GGV in active and completed panels.

| A-A case: (active panel; advancing face) | |
|---|---|
| Parameter | Min; mean; max |
| Distance to SC top (ft) | (878.5; 1155.4; 1419.2) |
| Surface elevation (ft) | (2095.0; 2502.7; 2855.4) |
| Average OB depth (ft) | (1296.0; 1499.7; 1743.9) |
| C-I case: (completed panel; idle face) | |
| Parameter | Min; mean; max |
| Distance to SC top (ft) | (966.3; 1190.5; 1423.5) |
| Surface elevation (ft) | (2197.3; 2499.9; 2803.2) |
| Average OB depth (ft) | (1338.6; 1503.7; 1700.7) |

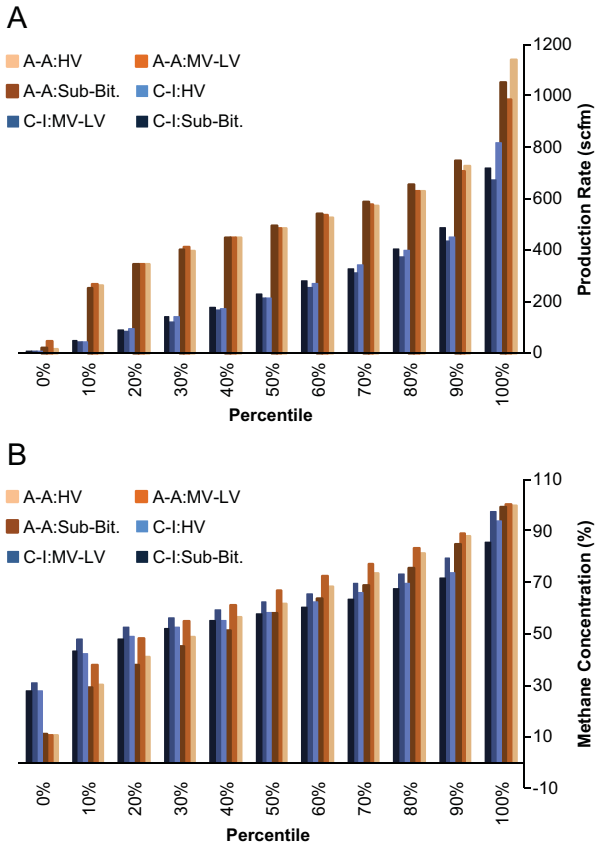


**Fig. 10.** Percentiles corresponding to different production rates (A) and methane percentage outputs (B) from conditional MC simulations using increased depths (Table 8) and the other parameters in Table 5.

**Table 9**
Tabulated percentiles of the data presented in Fig. 10.

A-A case: (active panel; advancing face)

| Coal rank | HV bit. coals | | MV–LV coals | | Sub-bit. coals | |
|---|---|---|---|---|---|---|
| Percentile | Prod. rate (scfm) | Methane (%) | Prod. rate (scfm) | Methane (%) | Prod. rate (scfm) | Methane (%) |
| 100% | 1137.38 | 99.7 | 986.19 | 100.0 | 1051.50 | 99.2 |
| 90% | 728.18 | 87.7 | 703.87 | 89.2 | 744.68 | 84.9 |
| **80%** | **629.79** | **81.0** | **626.74** | **83.5** | **654.30** | **75.6** |
| 70% | 572.05 | 73.7 | 576.87 | 77.1 | 589.47 | 68.8 |
| 60% | 525.25 | 68.1 | 533.82 | 72.6 | 542.33 | 63.8 |
| **50%** | **481.46** | **61.7** | **483.81** | **66.7** | **491.89** | **58.0** |
| 40% | 445.42 | 56.3 | 446.70 | 60.9 | 450.15 | 51.4 |
| 30% | 396.43 | 48.5 | 410.91 | 55.0 | 402.14 | 45.0 |
| **20%** | **343.01** | **41.0** | **346.38** | **48.0** | **346.72** | **37.7** |
| 10% | 260.08 | 30.1 | 265.40 | 37.7 | 250.50 | 29.0 |
| 0% | 13.90 | 10.7 | 46.45 | 10.7 | 21.66 | 10.9 |

C-I case: (completed panel; idle face)

| Coal rank | HV bit. coals | | MV–LV coals | | Sub-bit. coals | |
|---|---|---|---|---|---|---|
| Percentile | Prod. rate (scfm) | Methane (%) | Prod. rate (scfm) | Methane (%) | Prod. rate (scfm) | Methane (%) |
| 100% | 817.73 | 93.9 | 672.94 | 97.4 | 718.53 | 85.7 |
| 90% | 451.11 | 73.6 | 436.42 | 79.4 | 488.99 | 71.7 |
| **80%** | **399.32** | **69.6** | **371.87** | **73.1** | **403.91** | **67.3** |
| 70% | 342.22 | 65.8 | 309.27 | 69.4 | 326.96 | 63.5 |
| 60% | 269.67 | 62.3 | 254.34 | 65.4 | 279.85 | 60.1 |
| **50%** | **213.56** | **58.3** | **213.33** | **62.2** | **230.81** | **57.8** |
| 40% | 173.12 | 55.2 | 167.12 | 59.4 | 177.39 | 55.0 |
| 30% | 139.68 | 52.3 | 121.84 | 56.4 | 140.95 | 52.3 |
| **20%** | **96.79** | **49.0** | **83.09** | **52.7** | **89.37** | **47.9** |
| 10% | 44.46 | 42.2 | 41.00 | 48.0 | 48.97 | 43.1 |
| 0% | 0.11 | 28.0 | 1.46 | 30.7 | 0.21 | 27.9 |

The numbers in bold correspond to 20%, 50% and 80% percentiles, which were selected as the low, mean and high values within the range.

for production rates and methane concentrations, respectively. The simulation percentile, production rate, and methane concentration data are given in Table 9. Production rates (Fig. 10-A) showed a drastic increase, especially for the A-A case, with the increased values of distance to slotted casing, surface elevation, and average overburden compared to Fig. 9-A. Comparing the percentile values in Table 9 to those in Table 7 shows that the rates were almost doubled. By contrast, Fig. 10-B shows only slight increases in methane concentrations for both A-A and C-I cases compared to the results with the lower range (Fig. 9-B).

## 5. Summary and conclusions

GGVs are integral to the safety of many underground longwall coal mines, but their performances are difficult to forecast and, as a result, it is a challenge to optimize their designs. The complex interactions between GGV operating parameters, mining operating parameters and a host of dynamic geologic conditions result in GGV performance data that are difficult to understand and model, making stochastic models a good choice for representing the data.

In this work, a set of deterministic models was derived using the previously developed Methane Control and Prediction (MCP) software suite. The input parameters were assessed and adjusted so that the models could be generalized to sites other than the northern Appalachian basin, where the field data were collected. Methane concentrations and production rates were generated using MCP with random input values from a realistic range. Multilinear regressions were performed on the data. Reasonable coefficients of determination ($R^2$), from 0.69 to 0.88, were obtained. Next, it was determined that slotted casing length, strata displacement, and gas content of the overlying strata were important parameters for generalizing the models away from site-specific data. Subsidence is difficult to generalize across many sites, but it is a parameter that can significantly influence gas production by increasing conductivity to other gas bearing seams. Under this more generalized model, strata displacement was considered instead, allowing for these mechanisms to be taken into account. Strata displacement was only considered over the length of the slotted casing, which is crucial because the slotted casing promotes collection of gas from these fractured strata. Their inclusion in the deterministic models resulted in coefficients of determination ranging from 0.69 to 0.89. Comparison of statistical data between the two deterministic models indicated good agreement, except for skewness in production rates. In both A-A and C-I cases, absolute value of the skewness decreased, representing a more normal distribution with the modified models.

Probability distributions for the input data were created for use in Monte Carlo simulations of the modified deterministic models presented above. The Kolmogorov–Smirnov (K–S) goodness-of-fit test determined that the distributions could be represented with normal and log-normal distributions. 5000 simulations for each of the coal ranks (HV, MV–LV and sub-bituminous) in each of the longwall cases (A-A and C-I) were run for a total of 30,000 simulations. Conditional arguments were then applied to the resulting data in order to check that input parameters and outputs were valid. Simulations with invalid parameters or outputs were removed from the dataset.

Analysis of the output from the Monte Carlo simulations indicated that overall production rates were generally higher for GGVs over completed, inactive (C-I) longwall panels, but that methane concentrations were likely to be slightly lower in the produced gas stream for C-I panels than for advancing, active (A-A) panels. Further, the results indicated that in the 20th to 70th percentile range for the C-I case,

methane concentration ranged from 50 to 60%, a relatively small variation. This indicates that changes in well operating parameters are not as important during the completed and idle phase of GGV production.

This research quantifies the likelihood of operating a GGV within a given range of production rates and methane concentrations, using a stochastic modeling method. This allows operators to quickly determine if GGVs are operating within normal ranges and to explore why they may operate outside of these ranges. These data can also be used for preliminary design of GGVs. The advantage of this method is that input parameters that cannot be accounted for in deterministic modeling are incorporated into the stochastic model, so that a more comprehensive model is generated. The detailed discussion of development of the stochastic model allows for the procedure to be transferred to specific sites or basins.

This work indicates that the stochastic approach is a promising method to represent the randomness in GGV performances and to improve the limited and site-specific character of deterministic models. Future work may include analyzing data from other basins to prove that this stochastic method can be generalized to other sites. The initial deterministic model may be improved to generate a more comprehensive data distribution for Monte Carlo simulation. The stochastic model presented here for forecasting GGV performance can be used both in design of longwall GGVs and in optimizing operating parameters of existing GGVs to more efficiently extract methane from working areas of underground mines.

*List of symbols*

| | |
|---|---|
| $P_i$ | Production parameters (listed in Table 1) |
| $x_i$ | Production parameter coefficients (listed in Table 1) |
| $R_i$ | Coefficients of determination (listed in Table 1) |
| $y_i$ | Methane concentration parameters (listed in Table 1) |
| FRF | Flow rate change factors |
| FP | Flow percent |
| OB | Overburden depth |
| D | Distance to the top of the slotted casing |
| SL | Slotted casing length |
| SD | Strata displacement |
| $\mu$ | Mean for normal and log-normal distributions |
| $\sigma$ | Standard deviation for normal and log-normal distributions |

*Conversion Table (English to SI units)*

1 ft = 0.3048 m

1 MMscf = 28316 $m^3$

1 scfm = 0.0004719 $m^3/s$

## References


Ades, A.E., Lu, G., 2003. Correlations between parameters in risk models: estimation and propagation of uncertainty by Markov Chain Monte Carlo. Risk Analysis 23, 1165–1172.

Alper, J.S., Gelb, R.I., 1990. Standard errors and confidence intervals in nonlinear regression: comparison of Monte Carlo and parametric statistics. Journal of Physical Chemistry 94, 4747–4751.

Chakravarti, I.M., Laha, R.G., Roy, J., 1967. Handbook of Methods of Applied Statistics, vol. I. John Wiley and Sons, pp. 392–394.

Devore, J., Peck, R., 2001. Statistics: the Exploration and Analysis of Data. Duxbury Thomson Learning Inc., Pacific Grove, California.

Diamond, W.P., Schatzel, S.J., 1998. Measuring the gas content of coal: a review. International Journal of Coal Geology 35, 311–331.

Diamond, W.P., La Scola, J.C., Hyman, D.M. 1986. Results of direct-method determination of the gas content of the US coalbeds. Information Circular No. 9067, US Dept. of Interior, US Bureau of Mines, Pittsburgh, PA.

Diamond, W.P., Ulery, J.P., Kravitz, S.J. 1992. Determining the source of longwall gob gas: Lower Kittanning Coalbed, Cambria County, PA. Bureau of Mines, Information Circular No: 9430.

Dougherty, H., Karacan, C.Ö., in press. A new methane control and prediction (MCP) software suite for longwall mines. Computers and Geosciences.

Esterhuizen, G., Karacan, C., 2007. A methodology for determining gob permeability distributions and its application to reservoir modeling of coal mine longwalls. 2007 SME Annual Meeting and Exhibit, Februrary 25–28, Denver, Colorado, preprint 07-78.

Haghighat, A., Wagner, J.C., 2003. Monte Carlo variance reduction with deterministic importance functions. Progress in Nuclear Energy 42, 25–53.

Huang, H., Hassan, A.E., Hu, B.X., 2003. Monte Carlo study of conservative transport in heterogeneous dual-porosity media. Journal of Hydrology 275, 229–241.

Karacan, C.Ö., 2008. Modeling and prediction of ventilation methane emissions of U.S. longwall mines using supervised artificial neural networks. International Journal of Coal Geology 73, 371–387.

Karacan, C.Ö., 2009a. Forecasting gob gas venthole production performances using intelligent computing methods for optimum methane control in longwall coal mines. International Journal of Coal Geology 79, 131–144.

Karacan, C.Ö., 2009b. Elastic and shear moduli of coal-measure rocks derived from basic well logs using fractal statistics and radial basis function networks. International Journal of Rock Mechanics and Mining Sciences 46, 1281–1295.

Karacan, C.Ö., 2009c. Degasification system selection for U.S. longwall mines using an expert classification system. Computers and Geosciences 35, 515–526.

Karacan, C.Ö., 2010. Methane control and prediction (MCP) software. http://www.cdc.gov/niosh/mining/products/product180.htm.

Karacan, C.Ö., Goodman, G.V.R., 2009. Hydraulic conductivity changes and influencing factors in longwall overburden determined by slug tests in gob gas ventholes. International Journal of Rock Mechanics and Mining Sciences 46, 1162–1174.

Karacan, C.Ö., Esterhuizen, G.S., Schatzel, S.J., Diamond, W.P., 2007. Reservoir simulation-based modeling for characterizing longwall methane emissions and gob gas venthole production. International Journal of Coal Geology. 71 (2–3), 225–245.

Kelsey, A., Lea, C.J., Lowndes, I.S., Whittles, D., Ren, T.X., 2003. CFD modelling of methane movement in mines. The 20th International Conference of Safety in Mines Research Institues, South African Institute of Mining and Metallurgy.

Lu, Z., Zhang, D., 2003. On the importance sampling Monte Carlo approach to uncertainty analysis for flow and transport. Advances in Water Resources 26, 1177–1188.

Lunarzewski, L., 1998. Gas emission prediction and recovery in underground coal mines. International Journal of Coal Geology 35, 117–145.

Maier, H.R., Dandy, G.C., 2000. Neural networks for the prediction and forecasting of water resources variables: a review of modeling issues and applications. Environmental Modeling and Software 15, 101–124.

Mazza, R.L., Mlinar, M.P., 1977. Reducing methane in coal mine gob areas with vertical boreholes. U.S. Department of Interior, Bureau of Mines Research Report No. 1607-1-77.

McKay, M.D., Beckman, R.J., Conover, W.J., 1979. A comparison of three methods for selecting values of input variables in the analyses of output from a computer code. Technometrics 21, 239–245.

Morin, A.M., Ficarazzo, F., 2006. Monte Carlo simulation as a tool to predict blasting fragmentation based on the Kuz–Ram model. Computers and Geosciences 32, 352–359.

Palchik, V., 2003. Formation of fractured zones in overburden due to longwall mining. Environmental Geology 44, 28–38.

Palchik, V., 2005. Localization of mining-induced horizontal fractures along rock layer interfaces in overburden: field measurements and prediction. Environmental Geology 48, 68–80.

Palchik, V., 2010. Experimental investigation of apertures of mining induced horizontal fractures. International Journal of Rock Mechanics and Mining Sciences 47, 502–508.

Ren, T.X., Edwards, J.S., 2002. Goaf gas modeling techniques to maximize methane capture from surface gob wells. In: De Souza, Euler (Ed.), Mine Ventilation, pp. 279–286.

Ripley, B.D., 1987. Stochastic Simulation. Wiley, New York.

Sari, M., 2009. The stochastic assessment of strength and deformability characteristics for a pyroclastic rock mass. International Journal of Rock Mechanics and Mining Sciences 46, 613–626.

Structured data, 2008. RiskAMP: risk analysis and modeling program. http://www.riskamp.com.

Tomita, S., Deguchi, G., Matsuyama, S., Li, H., Kawahara, H., 2003. Development of a simulation program to predict gas emission based on 3D stress analysis. 30th International Conference of Safety in Mines Research Institutes, South African Institute of Mining and Metallurgy, pp. 69–76.

Vose, D., 2000. Risk Analysis: a Quantitative Guide, 2nd Ed. Wiley, Chichester.